

# Enhanced heat stability and storage modulus in novel PTMO-intercalated clay platelets/PTMO-based polyurethane nanocomposites

Hossein Behniafar<sup>1</sup> · Aziz Ahmadi-khaneghah<sup>1</sup> · Mojtaba Yazdi<sup>1</sup>

Received: 16 May 2016 / Accepted: 22 August 2016 / Published online: 26 August 2016  
© Springer Science+Business Media Dordrecht 2016

**Abstract** Amine-telechelic poly(tetramethylene oxide) (PTMO) was trimethylated to a quaternary ammonium (QA)-capped PTMO as a bivalent organic macrocation. This QA-capped PTMO (QAPTMO) was used for intercalation of montmorillonite (MMT) platelets with 69 % ion exchange yield and 4.03 nm *d*-spacing. Then, segmented polyurethanes (SPU) with PTMO soft segments were synthesized in the presence of the QAPTMO-intercalated MMT filler in different contents. According to the X-ray and SEM analyses, the polyaddition reaction could result in a full exfoliation of the clay platelets. Two model composites including SPU polymer loaded by unmodified MMT and tetradecyltrimethylammonium bromide (TTAB)-intercalated MMT were also synthesized analogously. The SPU/QAPTMO-MMT composites possessing 5.0 and 7.0 wt.% of the filler obviously showed a better thermal behavior in comparison with SPU/TTAB-MMT and SPU/Na-MMT composites. In addition, a significant increase in the storage moduli of the polyurethane matrices occurred due to the QAPTMO-MMT particles, particularly in the 5.0 wt.% loading content of the filler.

**Keywords** Polymer-matrix composites · Montmorillonite · Intercalation · Thermal analysis · Dynamic mechanical analysis · Electron microscopy

**Electronic supplementary material** The online version of this article (doi:10.1007/s10965-016-1097-z) contains supplementary material, which is available to authorized users.

✉ Hossein Behniafar  
h\_behniafar@du.ac.ir

<sup>1</sup> Faculty of Chemistry, Damghan University, Damghan 36715-364, Iran

## Introduction

Among various kinds of inorganic fillers, layered silicates have been extensively studied in preparing polymer-matrix composites due to their high reinforcing capability even at very low contents [1–6]. However, this kind of fillers has so hydrophilic character, and need to be organically modified by an appropriate organifier prior to use. This organo-modification causes an increase in interlayer spaces of the clay mineral, further helping the polymer chains, or monomers, to diffuse into the platelets. In fact, this facilitates the process for achieving a uniform polymer-clay nanocomposite with fully exfoliated clay platelets. This modification is generally based on a cationic exchange reaction between the inorganic cations of clay and the organocations of the modifier; usually ammonium [7–11] or phosphonium [12–15] ions of an appropriate emulsifier. It is expected that the dispersion of these homogeneously exfoliated nanolayers into various kinds of polymer matrices can improve thermo-mechanical properties of the resulting material.

On the other hand, segmented polyurethanes (SPU's) such as those of prepared from poly(tetramethylene oxide) (PTMO) and methylene diphenyl diisocyanate (MDI) or toluene diisocyanate (TDI) have been widely used in the field of polymer-matrix composites [16–20]. For instance, PTMO-based SPU's loaded by exfoliated clay platelets have been prepared, and their biocompatibility and antimicrobial activities investigated [21]. Recently, we reported synthesis and thermo-mechanical behavior of some PTMO-derived SPU's incorporated by organically modified silica and titania nanoparticles [22, 23]. In this work, PTMO-modified montmorillonite (MMT) platelets are loaded into PTMO-based SPU's during the synthesis process, leading to a novel class of SPU/clay nanocomposites. The clay platelets are initially intercalated by bivalent ammonium salt of PTMO prior to their exfoliation by the in-situ resulting SPU macromolecules. Herein, PTMO is

used both as macromonomer of the polyaddition reaction, responsible for creating soft segments of the resulting polyurethanes and as the intercalating agent for enhancing the clay interlayer space after its conversion to the corresponding quaternary ammonium (QA) salt. Structural similarity between the organic bivalent macrocations (QA-capped PTMO), which participate in the ion-exchange process and the soft segments of the polymer chains allows the chains to laminate easily the MMT platelets. In this condition the PTMO-intercalated nanolayers could be homogeneously exfoliated by PTMO-based polyurethane chains. The resulting samples are characterized by Fourier transform infrared (FTIR), X-ray diffraction (XRD), and scanning electron microscopy (SEM) techniques. Thermal stability and storage moduli ( $E'$  values) of the resulting nanocomposites are also investigated by thermogravimetric analysis (TG/DTG) and dynamic mechanical thermal analysis (DMTA) measurements.

## Experimental

### Materials

Flake-like 4,4'-methylenediphenyl diisocyanate (98 %) (MDI) was supplied by Acros Organics Co., and used as received. Other reactants involving hydroxyl telechelic PTMO (PTHF1000), 1,4-butanediol ( $\geq 99$  %) (BDO), thionyl chloride (99 %), potassium phthalimide ( $\geq 99$  %), hydrazine hydrate, methyl iodide ( $\geq 99.5$  %), and tetradecyltrimethylammonium bromide (99 %) (TTAB) were purchased from Merck Co. and used without further purification. N,N-Dimethylformamide (99.5 %) (DMF), toluene ( $>99$  %), dichloromethane ( $\geq 99$  %) (DCM), and diethyl ether ( $>96$  %) (DEE) were also obtained from Merck Co., and thoroughly dehydrated prior to use. Sodium montmorillonite (Na-MMT) with cation exchange capacity (CEC) of 92.6 meq/100 g was obtained from Southern Clay Products Inc.

### Measurements

FTIR spectra of the samples were recorded on a PERKIN ELMER RX I FTIR spectrophotometer. The spectra of solids were obtained using KBr pellets. To measure the  $d$ -spacing values, XRD patterns were conducted at room temperature with montmorillonite powders and polyurethane films on a Bruker-D8 Advance X-ray diffractometer with Ni-filtered  $\text{Cu}/\text{K}\alpha$  radiation (30 kV, 25 mA), and  $\lambda = 1.5406 \text{ \AA}$  in the angular range of  $2\theta = 0\text{--}10^\circ$ . HITACHI S-4160 Microscope was used for SEM at an acceleration voltage of 15 kV. Prior to the capturing, the samples were attached to double-sided carbon tape and coated with 100 nm gold using a DC sputtering coater. TG/DTG were performed on a Simultaneous Thermal Analyzer STA 503 under argon atmosphere at a heating rate of  $10 \text{ }^\circ\text{C}/\text{min}$  in the thermal range of  $25\text{--}600 \text{ }^\circ\text{C}$  with  $\text{Al}_2\text{O}_3$  as a

reference to measure the ion exchange fraction of organoclay and the thermal stability of polyurethane and polyurethane/clay nanocomposites. DMTA were measured by using a TT DMA Triton Technology, and the tests were conducted under nitrogen blanket by quenching the samples from ambient temperature to  $-75 \text{ }^\circ\text{C}$  and thereafter heating them under a frequency of 1 Hz at a rate of  $3 \text{ }^\circ\text{C}/\text{min}$ .

### Four-step synthesis of QA-capped PTMO

- Cl-PTMO-Cl synthesis: A solution of HO-PTMO-OH (20.045 g, 20 mmol) in toluene (120 mL) was poured into a flask equipped with a magnetic stirrer, a Dean-Stark trap, and a reflux condenser. The solution was stirred and refluxed until no more water was azeotropically collected in the trap. After cooling to room temperature, pyridine (3.24 mL, 40 mmol) was added to the flask in one portion. The mixture was reheated to reflux temperature and then thionyl chloride (8.78 mL, 120 mmol) added dropwise during 1 h, while stirring. It was remained in this condition for another 5 h, and then allowed to be cooled to room temperature. The pyridinium hydrochloride formed was filtered off, and the filtrate was concentrated to a viscose brown liquid. The product was dissolved in a DCM solvent saturated by anhydrous  $\text{K}_2\text{CO}_3$ , the solids were filtered off again, and the solvent of the filtrate evaporated completely to give the pure chlorinated PTMO (18.865 g, 91 % yield).
- $\text{Ph}(\text{CO})_2\text{N-PTMO-N}(\text{CO})_2\text{Ph}$  synthesis: Into a 250-mL round-bottom flask fitted by a reflux condenser and a nitrogen inlet, a solution of Cl-PTMO-Cl (18.038 g, 18 mmol) and potassium phthalimide (25.749 g, 139 mmol) in DMF solvent (120 mL) was heated to  $125 \text{ }^\circ\text{C}$ , and magnetically stirred for 5 h under nitrogen flow. After cooling, the reaction mixture was filtered, and the filtrate was concentrated in vacuo to yield a light yellow liquid. To remove the residue KCl impurities, the resulting crude product was dissolved in DCM. After filtration of the obtained mixture, the filtrate was concentrated to give a viscose liquid, i.e. phthalimide-terminated PTMO (16.758 g, 72 % yield).
- $\text{H}_2\text{N-PTMO-NH}_2$  synthesis: The imide-functionalized PTMO (16.012 g, 12 mmol) and hydrazine hydrate (18.63 mL, 384 mmol) were dissolved in absolute ethanol (120 mL), and poured into a reaction flask equipped with a reflux condenser and a nitrogen inlet. Next, the mixture was refluxed for 20 h under nitrogen flow, while stirring. After cooling, phthalhydrazide byproduct was filtered off in vacuo, and the ethanol evaporated in full to obtain an oily solid. This raw product was dissolved in DCM, filtered, and then reprecipitated in a large excess amount of DEE to give pure aminated PTMO (13.980 g, 86 % yield) as a butter-like yellow solid.
- $\Gamma(\text{CH}_3)_3\text{N}^+\text{-PTMO-N}^+(\text{CH}_3)_3\Gamma$  synthesis: Into a 250-mL round-bottomed flask a mixture containing the previously

synthesized  $H_2N$ -functionalized PTMO (13.025 g, 13 mmol), iodomethane (8.01 mL, 130 mmol), and anhydrous  $K_2CO_3$  (8.983 g, 65 mmol) in EtOAc (100 mL) was magnetically stirred at room temperature for 24 h. The reaction mixture was then filtered at reduced pressure, and the solids obtained were thoroughly washed with EtOAc ( $2 \times 50$  mL). Next, the crude product was dissolved in absolute EtOH (500 mL), and then the mixture was filtered again for removal of  $K_2CO_3$  impurities. Finally, the solvent of the filtrate evaporated completely in vacuo to afford pale yellow solids of QA-capped PTMO (9.982 g, 54 % yield) with melting point of 308 °C.

### Intercalation of Na-MMT by QA-capped PTMO

Na-MMT powder (1.625 g) was dispersed in deionized water (150 mL), and then vigorously stirred overnight. To destroy the residue agglomerates, the resulting suspension was also kept in an ultrasonic bath at room temperature for 1 h. A 500-mL round-bottomed flask containing 300 mL deionized water was charged with the prepared suspension, and stirred magnetically at 80 °C for another 45 min. A solution of QA-capped PTMO (1.045 g, 48 mmol) (2 CEC) in deionized water (30 mL) was added to the flask dropwise within 10 min, while stirring. The cation exchange process was allowed to be completely carried out for 72 h with the same conditions. The mixture was then filtered, and the solid obtained was thoroughly washed with deionized water (300 mL). The organically modified montmorillonite (QAPTMO-MMT) was dried in a vacuum oven at 80 °C for 12 h. To compare the results, a reference sample involving montmorillonite modified by TTAB instead of QAPTMO was also prepared by a similar manner.

### Exfoliation of PTMO-intercalated platelets by PTMO-based SPU

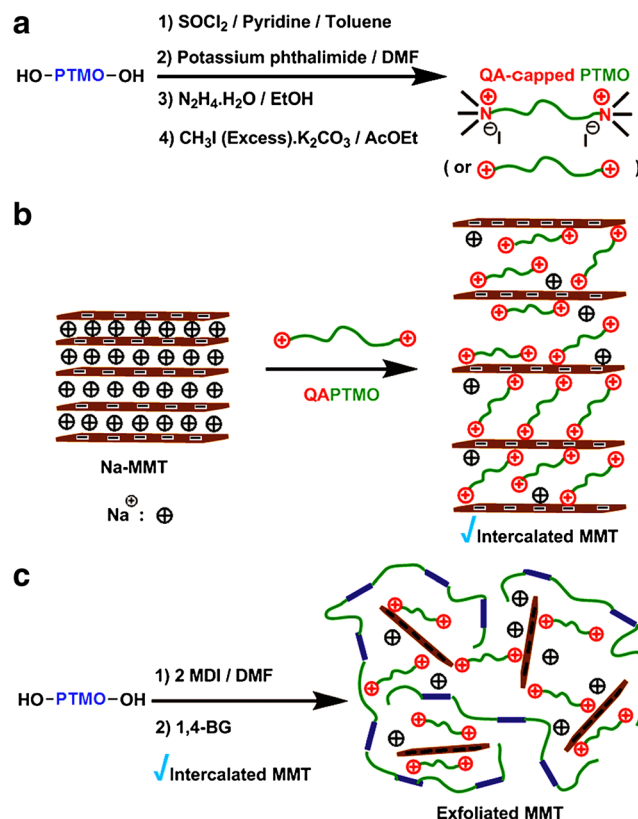
A 100-mL round-bottomed flask equipped with a mechanical stirrer, a thermometer, a reflux condenser, and a nitrogen inlet was charged by a solution of MDI (3.012 g, 12 mmol) and PTMO (6.020 g, 6 mmol) in DMF (30 mL). The solution was heated to 90 °C, and stirred mechanically at this temperature for 2.5 h under nitrogen stream. Then, while vigorously stirring, 1,4-BG (0.53 mL, 6 mmol) was added to the reaction flask, and the mixture remained with the same conditions for additional 10 min. On the other hand, QAPTMO-modified montmorillonite powders (2.5, 5.0, and 7.0 wt.% with respect to the target polymer) were sonically dispersed in DMF (5 mL) for 1 h, and then added to the flask. Thereafter, it was allowed to be stirred for 3 h at room temperature to obtain a highly viscous solution. To prepare the corresponding polyurethane films, the solution was subsequently poured into 9-cm glass Petri dishes. The transparent films with high

flexibility could be obtained at 70 °C for 24 h. Two reference composites loaded by TTAB-organified and unmodified montmorillonite powders (5.0 wt.% for each) as well as a neat polyurethane were also synthesized analogously.

## Results and discussion

### Synthesis process

QA-capped PTMO (QAPTMO) was synthesized through a four-step reaction starting from hydroxyl-telechelic PTMO. This bivalent organic salt was obtained from trimethylation reaction of amine-terminated PTMO. The  $H_2N$ -PTMO- $NH_2$  was prepared from PTHF1000 similar to the method described by Wang et al. for preparing amine-terminated polyethylene oxide [24]. PTHF1000 was converted to the corresponding macrodiamine and then to QAPTMO with passing through Cl-PTMO-Cl and  $Ph(CO)_2N$ -PTMO- $N(CO)_2Ph$  precursors. The four-step reaction to achieve QAPTMO organifier is shown in Scheme 1(A). The resulting QAPTMO was then utilized as a new intercalating agent for montmorillonite platelets (Scheme 1(B)). It is expected that this bivalent macrocation can



**Scheme 1** The four-step reaction to QA-capped PTMO (a), intercalation of MMT platelets by QAPTMO (b), and exfoliation of the PTMO-intercalated platelets by PTMO-based SPU (c)

significantly enhance the organophilicity of the inorganic nanolayers along with a remarkable increase in their basal spacing. This will be possible through diffusion of QAPTMO into the montmorillonite platelets and exchange with the sodium ions present in the clay galleries. In this situation, if these PTMO-intercalated nanolayers are present in a medium that a polymer is being synthesized, the resulting macromolecules get a high capacity to incorporate into the nanolayers. This can reasonably lead to a full exfoliation of the organoclay platelets into the polymer matrix. Accordingly, as an exceptional choice, PTMO-based segmented polyurethanes were examined for this synthesis. The bivalent macrocations of QAPTMO loaded into the montmorillonite platelets and the soft segments of the SPU macromolecules both comprise tetramethylene oxide units in their structures. This equality allows the polyurethane chains and the intercalating agent to approach each other, resulting in

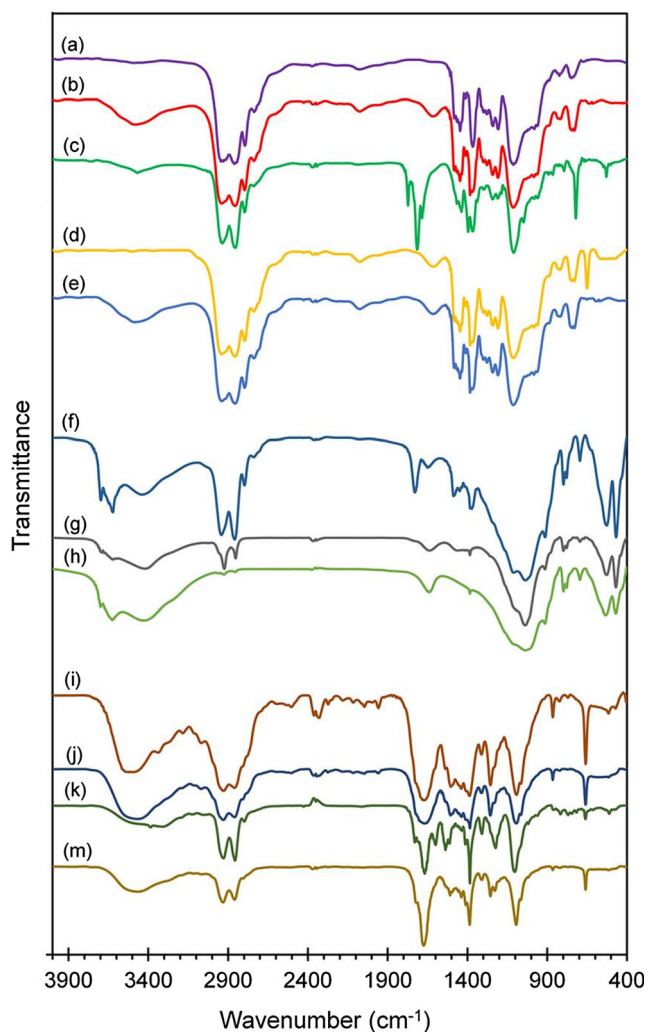


**Fig. 1** IR spectra of QAPTMO organifier (a),  $H_2N$ -telechelic PTMO (b),  $Ph(CO)_2N$ -PTMO- $N(CO)_2Ph$  (c), Cl-telechelic PTMO (d), HO-telechelic PTMO (e), QAPTMO-MMT (f), TTAB-MMT (g), Na-MMT (h), SPU/QAPTMO-MMT 7.0 % (i), SPU/TTAB-MMT 5 % (j), SPU/Na-MMT 5 % (k), and neat SPU (m)

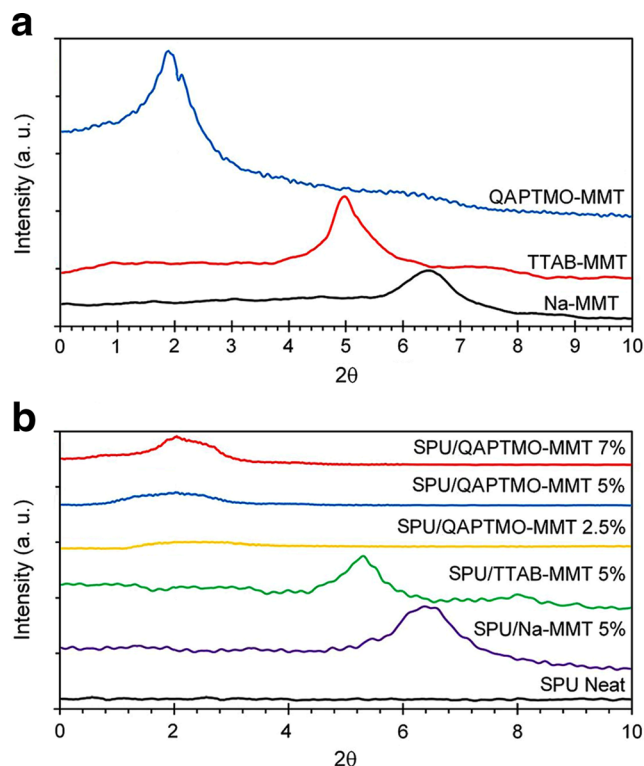


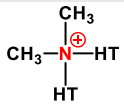
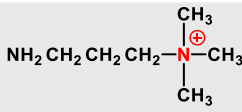
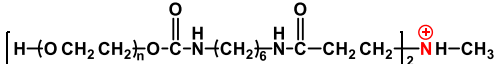
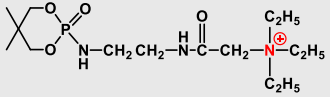
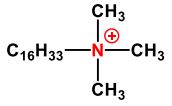
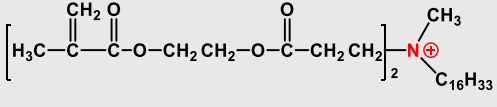
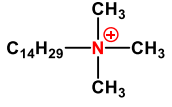
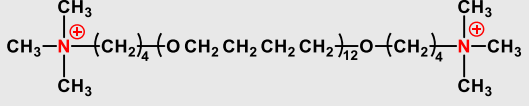
**Fig. 2** XRD profiles of clay particles (a) and the resulting SPU/clay nanocomposites (b)

a further dispersion of the nanolayers. Schematic illustration of the two-step polyaddition reaction for preparing PTMO-based SPU, which is being loaded by PTMO-intercalated MMT particles, is presented in Scheme 1(C). According to the formulation used for the polyaddition reactions, the hard/soft segments can lead to the weight ratio of 3/5 in the resulting SPU chains (~600 g for the molar weight of 2MDI + BDO as the hard segments vs. ~1000 g for the molar weight of PTMO as the soft segments). Here, PTMO has a dual role; both is used for intercalation of clay platelets in the form of its ammonium salt and is responsible for formation of the soft segments of the SPU chains. To compare the results, an intercalating agent other than QAPTMO, i.e. TTAB, was also utilized by a similar manner. In addition, two other references involving polyurethane loaded by Na-MMT as well as neat polyurethane were also synthesized.

Figure 1 shows the IR spectra of QAPTMO organifier (a) and all precursors (b-e) in the four-step reaction path. In the spectrum of the QA-capped PTMO, the N-H stretch peak of  $H_2N$ -PTMO- $NH_2$  centered at about  $3480\text{ cm}^{-1}$  thoroughly disappeared. In the spectra of QAPTMO-intercalated MMT (QAPTMO-MMT) (f) and TTAB-intercalated MMT (TTAB-MMT) (g) the peaks related to C-H stretch at  $2860$  and  $2945\text{ cm}^{-1}$  were added to the peaks of Na-MMT spectrum (h). The spectra of SPU/QAPTMO-MMT (7.0 wt.%) (i), SPU/TTAB-MMT (5 wt.%) (j), and SPU/Na-MMT (5 wt.%) (k) and the neat polyurethane (m) were also presented. In these spectra, the characteristic peaks attributed to the loaded clay,



**Table 1**  $2\theta$  and  $d$ -spacing values of various kinds of MMT particles

Organifier	$2\theta$ ( $^{\circ}$ )	$d_{001}$ (nm)	Ref.
None (Cloisite Na <sup>+</sup> )	7.1	1.17	[26]
 (Cloisite 15Å) HT: Hydrogenated Tallow	2.6	3.15	[27]
	6.2	1.35	[28]
	3.9	2.29	[29]
	4.5	1.94	[30]
	4.4	1.96	[31]
	4.2	2.05	[31]
 (TTAB)	4.9	1.80	
 (QAPTMO)	2.2	4.03	

which appear below  $650\text{ cm}^{-1}$  (470 and 516 for SPU/QAPTMO-MMT) could be observed.

### Structure and morphology

XRD technique provides information on the changes of the interlayer spacing of the organically modified MMT upon the formation of a nanocomposite. The formation of an intercalated structure should result in a decrease in  $2\theta$ , indicating an increase in the  $d$ -spacing. Hence, QAPTMO-intercalated MMT and PTMO-based SPU/organoclay nanocomposites were analyzed by XRD measurements, and compared with the corresponding reference samples. Figure 2a shows the

X-ray diffractograms of QAPTMO-MMT, TTAB-MMT, and Na-MMT. Upon intercalation of the clay platelets by QAPTMO organifier, a significant increase in the basal spacing occurred. The  $d$  spacing increased from 1.30 nm ( $2\theta = 6.6^{\circ}$ ) for Na-MMT to 4.03 nm ( $2\theta = 2.2^{\circ}$ ) for QAPTMO-MMT. This 2.73-nm enhancement clearly shows that a large amount of the organifier has been intercalated into the clay nanolayers. In this condition, the reference organifier, TTAB, increased the basal spacing of the pristine clay only 0.5 nm ( $2\theta = 4.9^{\circ}$ ). In addition to TTAB-MMT, some other organoclays have been compared with QAPTMO-MMT from  $2\theta$  value and basal spacing point of view (Table 1). According to the data of Table 1, it is clear that the basal spacing for QAPTMO-

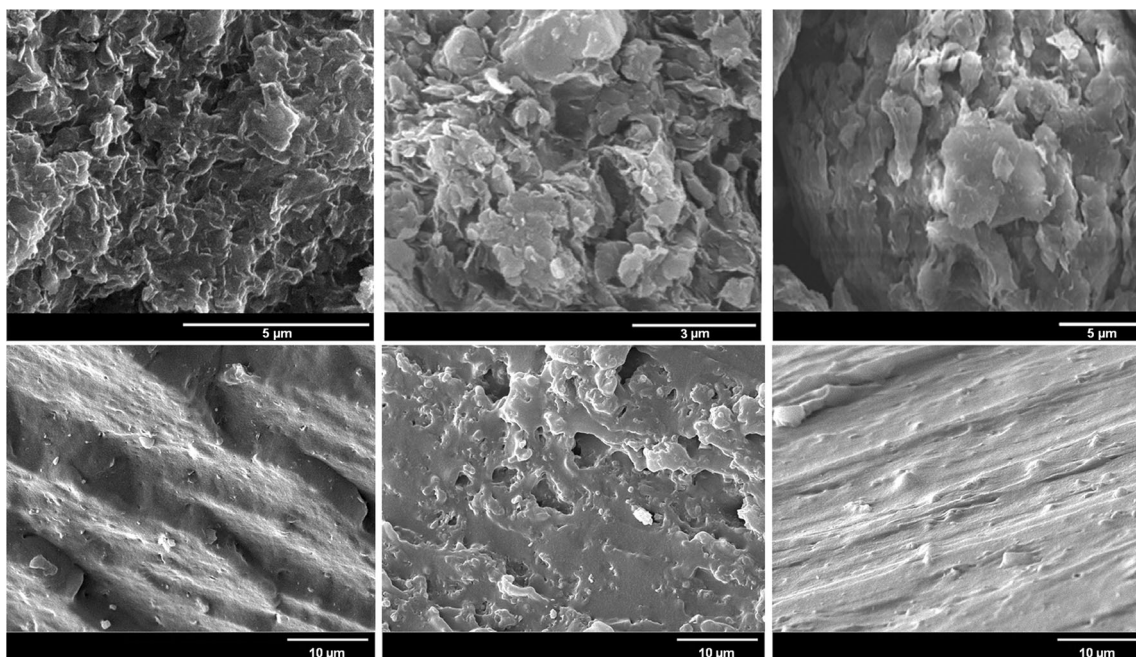


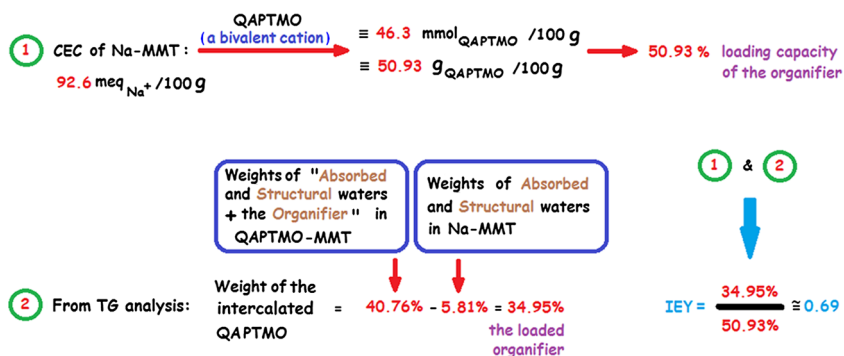
**Fig. 3** SEM images of QAPTMO-MMT (upper row, left side image), TTAB-MMT (upper row, middle image), Na-MMT (upper row, right side image), SPU/QAPTMO-MMT 2.5 % (lower row, left side image), SPU/

QAPTMO-MMT 7.0 % (lower row, middle image), and SPU/TTAB-MMT 5.0 % (lower row, right side image)

MMT is greater than the other organifiers. The characteristic peak associated with the clays (Na-MMT, TTAB-MMT, and QAPTMO-MMT) could be seen in the X-ray diffractograms of all clay-containing SPU composites as well (Fig. 2b). However, in the SPU/QAPTMO-MMT series (2.5, 5.0, and 7.0 %) this characteristic peak is obviously shorter and wider than those of the other two counterparts. This arises from the exfoliation of the clay platelets, since the formation of an exfoliated structure usually results in the complete loss of registry between the clay layers so that even no peak may be observed in the XRD trace [25]. When the regularity in the parallel nanolayers of expandable clay is disturbed due to an exfoliation process, the correlation between them as well as their reciprocal effectiveness is lowered, and their crystalline nature is highly destroyed. As a result, after exfoliation process in the XRD patterns, the sharp crystalline peaks of the nanolayers are converted to short and wide amorphous peaks.

Figure 3 displays the SEM images of the clay particles (upper row) and the SPU/clay composites (lower row). The images clearly show that both organifiers in particular QAPTMO caused the condensed platelets of Na-MMT to be relatively separated from each other. A significant intercalation of MMT by QAPTMO intercalating agent gave the clay particles a rock-like micrograph. On the other hand, as the images of the lower row show, the platelets of QAPTMO-MMT are easily observed within the resulting SPU matrix. When the micrographs of SPU/QAPTMO-MMT 2.5 % (left, bottom) and SPU/QAPTMO-MMT 7.0 % (middle, bottom) are compared with each other, it could be found that the surface morphology of the polymer matrix is significantly affected by the loading content of the organoclay particles. In addition, it seems that exfoliation of the clay nanolayers in SPU/QAPTMO-MMT (middle, bottom) is higher than that of SPU/TTAB-MMT 5 % (right, bottom).

**Fig. 4** The calculations associated with ion exchange yield (IEY) of organoclay particles



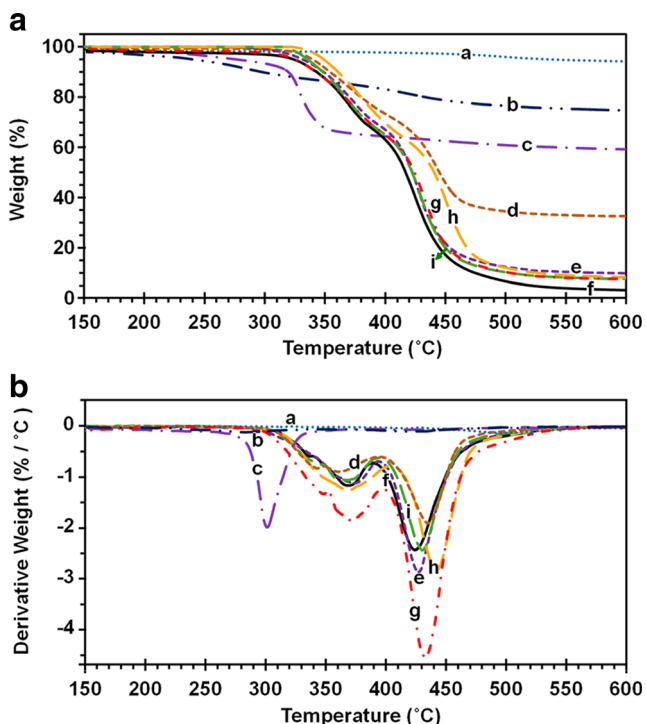


**Fig. 5** TG (a) and DTG (b) thermograms of clay particles and the resulting SPU/clay nanocomposites. (a) Na-MMT (b) TTAB-MMT (c) QAPTMO-MMT (d) SPU/QAPTMO-MMT 7 % (e) SPU/Na-MMT 5 % (f) SPU Neat (g) SPU/QAPTMO-MMT 2.5 % (h) SPU/QAPTMO-MMT 5 % (i) SPU/TTAB-MMT 5 %

**Thermal properties**

TG analyses were performed to measure the ion exchange yield (IEY) of organoclay as well as the thermal stability of organoclay-loaded polyurethane nanocomposites. The IEY is defined as the ratio of the loaded organifier to the maximum loading capacity. According to the calculations shown in Fig. 4, the IEY of QAPTMO was found to be 0.69. This means that about 69 % of sodium cations present in the layered silicate were replaced by the organifier via cation exchange process. Despite the high molecular weight of the organifier, QAPTMO showed relatively a high IEY value. Such

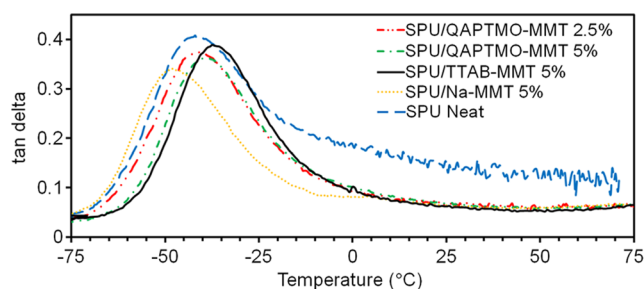


**Fig. 6** Tan  $\delta$  vs temperature for organoclay-loaded SPU composites along with the curves of two model samples including SPU/Na-MMT and neat SPU

calculations for the reference intercalating agent, TTAB, led to IEY value of 0.60.

Incorporation of the QAPTMO macrocations into the MMT nanolayers causes a significant increase in the basal spacing, which this in turn, facilitates their exfoliation during the polymerization stage. In addition, according to the hard-soft acid-base (HSAB) concept, the linkage of the ammonium hard ions with the strongly soft iodide counterions in QAPTMO is weaker than that of the bromide counterions in TTAB, which this makes the ion dissociation in QAPTMO easier. Figure 5 exhibits the thermal behavior of the QAPTMO-intercalated MMT and the resulting organoclay-loaded SPU nanocomposites together with the reference samples. The residue weights at 600 °C for Na-MMT, TTAB-MMT, and QAPTMO-MMT particles were found to be 94.20 %, 74.8 %, and 59.2 %, respectively. On the other hand, the thermal degradation of polyurethanes occurs in two stages: the first stage (~30 % weight loss) is mainly governed by the degradation of the hard segments and the second stage (~50 % weight loss) correlates well with the degradation of the soft segments [32]. This two-stage degradation is fully in agreement with the hard/soft weight ratio (3/5, as stated earlier) of the original formulation. Some results including the temperature of 5.0 wt.% degradation ( $T_{d5\%}$ ), the temperatures of maximum decomposition rate for the first and second stages ( $T_{max1}$  and  $T_{max2}$ ), and the char yields at 600 °C are shown in Table 2. In general, the clay platelets particularly in SPU/

**Table 2** Some thermal data of the resulting SPU/clay nanocomposites

Entry	Code	$T_{d5\%}$ <sup>a</sup> (°C)	$T_{max1}$ <sup>b</sup> (°C)	$T_{max2}$ <sup>c</sup> (°C)
1	SPU/QAPTMO-MMT (2.5 %)	335.5	368.8	430.1
2	SPU/QAPTMO-MMT (5.0 %)	348.9	370.3	441.5
3	SPU/QAPTMO-MMT (7.0 %)	339.6	360.9	434.4
4	SPU/TTAB-MMT (5.0 %)	325.0	370.5	432.6
5	SPU/Na-MMT (5.0 %)	331.5	374.1	427.0
6	SPU (neat)	323.9	369.9	424.3

<sup>a</sup> Temperature of 5.0 wt.% decomposition

<sup>b</sup> Temperature of maximum decomposition rate for the first stage

<sup>c</sup> Temperature of maximum decomposition rate for the second stage

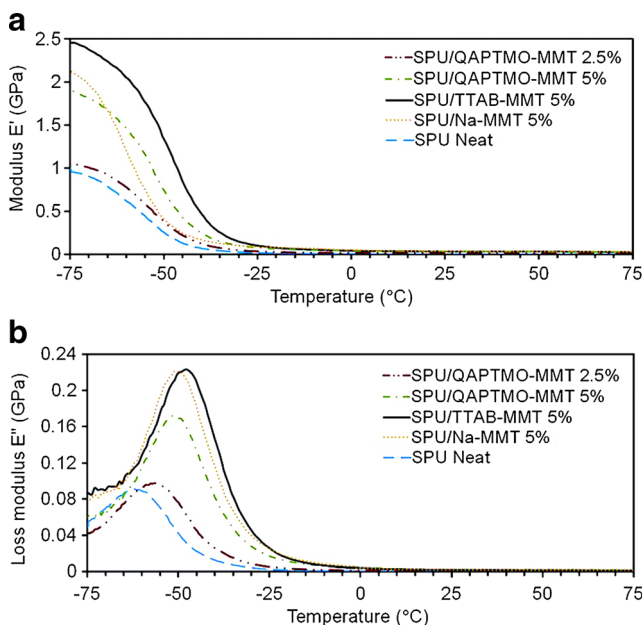


**Fig. 7** Storage modulus  $E'$  (a) and Loss modulus  $E''$  (b) vs temperature for some SPU/clay nanocomposites

QAPTMO-MMT 7.0 % nanocomposite could enhance the thermal stability. SPU/QAPTMO-MMT 5.0 % nanocomposite clearly exhibited a better thermal stability than the SPU/TTAB-MMT 5.0 % counterpart. This is due to the more homogeneous dispersion of QAPTMO-MMT platelets within the SPU matrix. Moreover, in the SPU/QAPTMO-MMT series, although the values of  $T_{d5\%}$ ,  $T_{max1}$  and  $T_{max2}$  for SPU/QAPTMO-MMT 5 % are greater than those of SPU/QAPTMO-MMT 7 %, based on the thermograms obtained the thermal behavior of the latter nanocomposite (SPU/QAPTMO-MMT 7 %) is better than that of the first one (SPU/QAPTMO-MMT 5 %). Therefore, according to the TG/DTG thermograms, the thermal stability of the SPU/QAPTMO-MMT series increases with increasing the filler content. The filler content up to 2.5 wt.% hasn't significant effect on the heat stability of the SPU/QAPTMO-MMT nanocomposites. However, when the content of QAPTMO-MMT filler increases up to 5.0 wt.%, the stability towards heat considerably increases. The filler plays the role of a thermal

insulator and mass transport barrier to the volatile products generated during decomposition [33].

### Dynamic mechanical thermal analysis

The temperature dependent  $\tan \delta$  responses of SPU/QAPTMO-MMT nanocomposites (two samples) and the related references are shown in Fig. 6. The peak of  $\tan \delta$  curve was determined as the glass transition temperature ( $T_g$ ) associated with the soft segments of the polymer. As the curves show, loading of the PTMO-based SPU samples by organically modified clay particles (QAPTMO-MMT and TTAB-MMT) shifts the polymer  $T_g$  to higher values. Conversely, unmodified MMT lowers the  $T_g$  value of the neat SPU possibly due to the creation of the filler aggregates within the polymer macromolecules, which this weakens the intermolecular interaction, and increases the chain mobility of the polymer. In addition, the  $T_g$  value increased with increasing the content of QAPTMO-MMT particles. This arises from the strong interactions due to the hydrogen bonding between the urethane groups of the polyurethane macromolecules and the oxygen atoms on the surface of the well dispersed silicate layers [34]. Moreover, the uniformity between the QA-capped PTMO intercalating agent and the PTMO soft segments of the polyurethane molecules helps these molecules to diffuse with high tendency inside the clay layers, leading to an efficient exfoliation of the platelets.

The curves of moduli (storage modulus  $E'$  and loss modulus  $E''$ ) vs temperature for pure SPU and SPU/organoclay nanocomposites are shown in Fig. 7. In comparison with the neat SPU, both moduli are obviously reinforced by loaded QAPTMO-MMT particles, in particular for the 5.0 wt.% loading. Also, thermo-mechanical reinforcements could be especially observed for the temperatures below the  $T_g$  values. However, SPU/QAPTMO-MMT (5.0 %) didn't show superior moduli compared to SPU/TTAB-MMT (5.0 %). This may be originated from the highly flexible structure of QAPTMO as the organifier of MMT platelets, which somewhat reduces the polymer resistance against the deformation. In general, the enhancement of modulus is reasonably attributed to the high resistance exerted by the MMT against the plastic/elastic deformation [35]. Moreover, comparison between the  $E'$  curves

**Table 3**  $T_g$  and two  $E'$  values of the resulting SPU/clay nanocomposites

Entry	Code	$T_g$ (°C)	$E'_{-75^a}$ (GPa)	$E'_{-45^b}$ (GPa)
1	SPU/QAPTMO-MMT (2.5 %)	-39.9	1.0	0.16
2	SPU/QAPTMO-MMT (5.0 %)	-39.0	1.8	0.31
3	SPU/TTAB-MMT (5.0 %)	-37.5	2.44	0.75
4	SPU/Na-MMT (5.0 %)	-47.8	2.1	0.25
5	SPU (neat)	-42.4	0.99	0.13

<sup>a</sup> Storage modulus at  $-75$  °C obtained from DMTA graphs

<sup>b</sup> Storage modulus at  $-45$  °C obtained from DMTA graphs



of SPU/QAPTMO-MMT (5.0 %) and SPU/QAPTMO-MMT (2.5 %) shows the storage modulus increases with increasing the filler content. Some results obtained from DMTA analyses including the glass transition temperatures and  $E'$  values at two temperatures below the  $T_g$ 's are summarized in Table 3.

## Conclusions

QA-capped PTMO was used as an exceptional intercalating agent of MMT nanolayers with 2.73 nm increase in the basal spacing of the pristine MMT. The intercalated nanolayers were then fully exfoliated by PTMO-based SPU macromolecules to prepare the corresponding thermally and thermomechanically reinforced polyurethane composites. The soft segments of the polymer and the diffused organifier were structurally equal, which undoubtedly this matter helped them to be close together. Consequently, a high degree of exfoliation of the clay platelets could be observed in this condition. SPU/QAPTMO-MMT nanocomposites showed superior thermal behavior compared to the model samples especially at higher temperatures. According to the DMTA profiles, the segmental motions in the SPU macromolecules were found to be even limited compared to the neat SPU sample due to the strong interactions between the homogeneously dispersed platelets and the soft segments of the SPU matrix. Furthermore, a significant enhancement occurred in the storage modulus of the polyurethane with loading by QAPTMO-MMT particles. Accordingly, QA-capped PTMO seems to be an excellent bivalent macro-organifier for intercalation of clay particles, which subsequently as a unique organoclay can be efficiently exfoliated by PTMO-based segmented polyurethanes.

**Acknowledgments** The authors wish to express their gratitude to the Faculty of Chemistry and Research Council of Damghan University for financial support of this research, and to Amirkabir University and University of Tehran for carrying out the DMTA and SEM analyses, respectively.

## References

1. Beall GW, Powell CE (2011) Engineering properties of polymer-clay nanocomposites theory and theory validation (Chapter 5) in: Fundamentals of polymer-clay nanocomposites. Cambridge University Press, New York
2. Chiu CW, Lin JJ (2012) Self-assembly behavior of polymer-assisted clays. *Prog Polym Sci* 37:406–444
3. Chiu CW, Huang TK, Wang YC, Alamani BG, Lin JJ (2014) Intercalation strategies in clay/polymer hybrids. *Prog Polym Sci* 39:443–485
4. Kiliaris P, Papispyrides CD (2010) Polymer/layered silicate (clay) nanocomposites: an overview of flame retardancy. *Prog Polym Sci* 35:902–958
5. Li M, Wu Z (2012) A review of intercalation composite phase change material: preparation, structure and properties. *Renew Sust Energ Rev* 16:2094–2101
6. Rafiemanzafat F, Adli V, Mallakpour S (2015) Effective preparation of clay/waterborne Azo-containing polyurethane nanocomposite dispersions incorporated anionic groups in the chain termini. *Des Monomers Polym* 18:303–314
7. Mallakpourea S, Shahangia V (2012) Modification of Clay with L-Leucine and TiO<sub>2</sub> with Silane Coupling Agent for Preparation of Poly(Vinyl Alcohol)/Organo-Nanoclay/Modified TiO<sub>2</sub> Nanocomposites Film. *Des Monomers Polym* 15:329–344
8. Zahra M, Zulfiqar S, Yavuz CT, Kweon HS, Sarwar MI (2014) Conductive nanocomposite materials derived from SEBS-g-PPy and surface modified clay. *Compos Sci Technol* 100:44–52
9. Jincheng W, Xiaoyu Z, Wenli H, Nan X, Xingchen P (2012) Synthesis of hyper-branched quaternary ammonium salt and its application into montmorillonite. *Powder Technol* 221:80–89
10. Huang Y-F, Wang P-C, Lee J-H, Lee J-Y, Liu H-J (2015) Crystallization and Thermal Properties of PLLA-PEG 600/Clay Nanocomposites. *Polym-Plast Technol Eng* 54:433–439
11. Shen Z, Cheng YB, Simon GP (2005) Sequential and Simultaneous Melt Intercalation of Poly(ethylene oxide) and Poly(methyl methacrylate) into Layered Silicates. *Macromolecules* 38:1744–1751
12. Cai Y, Hu Y, Xiao J, Song L, Fan W, Deng H, Gong X, Chen Z (2007) Morphology, Thermal and Mechanical Properties of Poly (Styrene-Acrylonitrile) (SAN)/Clay Nanocomposites from Organic-Modified Montmorillonite. *Polym-Plast Technol Eng* 46:541–548
13. Ezquerro CS, Ric GI, Minana CC, Bermejo JS (2015) Characterization of montmorillonites modified with organic divalent phosphonium cations. *Appl Clay Sci* 111:1–9
14. Suin S, Khatua BB (2012) Exfoliated and optically transparent polycarbonate/clay nanocomposites using phosphonium modified organoclay: preparation and characterizations. *Ind Eng Chem Res* 51:15096–15108
15. Mousa MH, Dong Y, Davies IJ (2016) Recent advances in bionanocomposites: preparation, properties, and applications. *Int J Polym Mater Polym Biomater* 65:225–254
16. Jomaa MH, Masenelli-Varlot K, Seveyrat L, Lebrun L, Dib Jawhar MC, Beyou E, Cavaille JY (2015) Investigation of elastic, electrical and electromechanical properties of polyurethane-grafted carbon nanotubes nanocomposites. *Compos Sci Technol* 121:1–8
17. Chattopadhyay DK, Webster DC (2009) Thermal stability and flame retardancy of polyurethanes. *Prog Polym Sci* 34:1068–1133
18. Jaoh D, Putson C, Muensit N (2016) Enhanced strain response and energy harvesting capabilities of electrostrictive polyurethane composites filled with conducting polyaniline. *Compos Sci Technol* 122:97–103
19. Liu X, Wang T, Li J, Cheng J, Zhang J (2015) Synthesis and properties of segmented polyurethanes with hydroquinone ether derivatives as chain extender. *J Polym Res* 22:149–159
20. Pokharel P, Choi S, Lee DS (2015) The effect of hard segment length on the thermal and mechanical properties of polyurethane/graphene oxide nanocomposites. *Compos A Appl Sci Manuf* 69:168–177
21. Tseng HJ, Lin JJ, Ho TT, Tseng SM, S-h H (2011) The biocompatibility and antimicrobial activity of nanocomposites from polyurethane and nano silicate platelets. *J Biomed Mater Res Part A* 99(A):192–202
22. Behniafar H, Azadeh S (2015) Transparent and flexible films of thermoplastic polyurethanes incorporated by Nano-SiO<sub>2</sub> modified with 4,4'-methylene diphenyl diisocyanate. *Int J Polym Mater Polym Biomater* 64:1–6
23. Behniafar H, Alimohammadi M, Malekshahinezhad K (2015) Transparent and flexible films of new segmented polyurethane nanocomposites incorporated by NH<sub>2</sub>-functionalized TiO<sub>2</sub> nanoparticles. *Prog Org Coat* 88:150–154

24. Wang L, Wang S, Bei JZ (2004) Synthesis and characterization of macroinitiator-amino terminated PEG and poly( $\gamma$ -benzyl-L-glutamate)-PEO-poly( $\gamma$ -benzyl-L-glutamate) triblock copolymer. *Polym Adv Technol* 15:617–621
25. Zheng X, Jiang DD, Wilkie CA (2006) Polystyrene nanocomposites based on an oligomerically-modified clay containing maleic anhydride. *Polym Degrad Stabil* 91:108–113
26. Mittal V (2014) Foams Based on Starch, Bagasse Fibers, and Montmorillonite (Chapter 4) in: *Polymer Nanocomposites Foams*. CRC Press, Boca Raton
27. Pegoretti A, Dorigato A, Brugnara M, Penati A (2008) Contact angle measurements as a tool to investigate the filler–matrix interactions in polyurethane–clay nanocomposites from blocked prepolymer. *Eur Polym J* 44:1662–1672
28. Nugay N, Nugay T, Kennedy JP (2013) Minute amounts of organically modified montmorillonite improve the properties of Polyisobutylene-based polyurethanes. *J Polym Sci Part A Polym Chem* 51:4076–4087
29. Choi WJ, Kim SH, Kim YJ, Kim SC (2004) Synthesis of chain-extended organifier and properties of polyurethane/clay nanocomposites. *Polymer* 45:6045–6057
30. Huang G, Gao J, Li Y, Han L, Wang X (2010) Functionalizing nano-montmorillonites by modified with intumescent flame retardant: preparation and application in polyurethane. *Polym Degrad Stabil* 95:245–253
31. Tan H, Ma G, Xiao M, Nie J (2009) Photopolymerization and characteristics of reactive organoclay–polyurethane nanocomposites. *Polym Composite* 30:612–618
32. Petrovic ZS, Zavargo Z, Flynn JH, Macknight WJ (1994) Thermal degradation of segmented polyurethanes. *J Appl Polym Sci* 51:1087–1095
33. Zanetti M, Camino G, Thomann R, Mulhaupt R (2001) Synthesis and thermal behaviour of layered silicate–EVA nanocomposites. *Polymer* 42:4501–4507
34. Ray SS, Okamoto K, Okamoto M (2003) Structure – Property relationship in biodegradable poly(butylene succinate)/layered silicate nanocomposites. *Macromolecules* 36:2355–2367
35. Nikolaidis AK, Achilias DS, Karayannidis GP (2012) Effect of the type of organic modifier on the polymerization kinetics and the properties of poly(methyl methacrylate)/organomodified montmorillonite nanocomposites. *Eur Polym J* 48:240–251